Exceptional Electrical Conductivity and Fracture Resistance of 3D Interconnected Graphene Foam/Epoxy Composites

Jingjing Jia,[†] Xinying Sun,[†] Xiuyi Lin,[†] Xi Shen,[†] Yiu-Wing Mai,[‡] and Jang-Kyo Kim[†,*]

[†]Department of Mechanical and Aerospace Engineering, The Hong Kong University of Science and Technology, Clear Water Bay, Kowloon, Hong Kong and [‡]Centre for Advanced Materials Technology (CAMT), School of Aerospace, Mechanical and Mechatronic Engineering J07, The University of Sydney, Sydney, NSW 2006, Australia

ABSTRACT Cellular-structured graphene foam (GF)/epoxy composites are prepared based on a three-step fabrication process involving infiltration of epoxy into the porous GF. The three-dimensional (3D) GF is grown on a Ni foam template *via* chemical vapor deposition. The 3D interconnected graphene network serves as fast channels for charge carriers, giving rise to a remarkable electrical conductivity of the composite, 3 S/cm, with only 0.2 wt % GF. The corresponding flexural modulus and strength increase by 53 and 38%, respectively, whereas the glass transition temperature increases by a notable 31 °C, compared to the solid neat epoxy. The GF/epoxy composites with 0.1 wt % GF also deliver an excellent fracture toughness of 1.78 MPa·m$^{1/2}$, 34 and 70% enhancements against their "porous" epoxy and solid epoxy counterparts, respectively. These observations signify the unrivalled effectiveness of 3D GF relative to 1D carbon nanotubes or 2D functionalized graphene sheets as reinforcement for polymer composites without issues of nanofiller dispersion and functionalization prior to incorporation into the polymer.

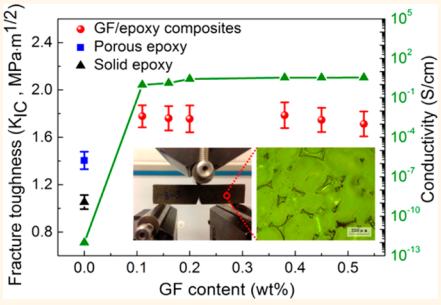

KEYWORDS: graphene foams · epoxy matrix composites · structure–property relationships · electrical conductivity · toughness · mechanical properties

Graphene has attracted tremendous attention due to its large surface area, high strength and Young's modulus, as well as extraordinary electronic properties and thermal conductivity.[1−3] As a precursor for graphene, graphene oxide (GO) enjoys an abundance of oxygenated functional groups on its surface which offer high processability and dispersibility in aqueous media. These properties make GO an ideal multifunctional nanofiller to prepare well-dispersed polymer nanocomposites with a tailored nanostructure and interphase. Pristine graphene, GO, and reduced graphene oxide (rGO) have been incorporated into a wide range of polymer matrices, including epoxy, polyurethane, polycarbonate, polystyrene, polyaniline, and poly(methyl methacrylate) (PMMA) to form composites possessing unique properties and capabilities.[4−9] However, there are a number of challenges that need to be addressed to maximize the reinforcement efficiency of graphene. Most importantly, the graphene nanosheets should be fully exfoliated and uniformly dispersed in the polymer to avoid reagglomeration, especially at high graphene contents, caused by the intermolecular $\pi-\pi$ stacking attraction forces.[10] Lack of exfoliation and dispersion of graphene sheets is always detrimental to achieving desired effects on mechanical, electrical, thermal, and other important properties. Another critical issue arising from the highly oxygenated GO sheets is that GO sheets ought to be reduced to recover the sp^2 carbon structure to restore the inherently high electrical conductivities of graphene and the composites made therefrom.[5,11]

GO sheets can be reassembled into free-standing thin films or paper-like materials *via* flow-directed assembly of aqueous dispersion,[12,13] which can offer a potentially useful route to fabricate exciting multifunctional nanocomposites. Nevertheless, processing bulk polymer composites using graphene papers as the reinforcement has

* Address correspondence to mejkkim@ust.hk.

Received for review January 29, 2014 and accepted May 21, 2014.

Published online May 21, 2014
10.1021/nn500590g

not been very successful to date due to the difficulties in intercalating polymer molecules into the stacked graphene sheets. As an alternative, efforts have been directed toward developing aligned graphene/polymer nanocomposites based on *in situ* solvent casting.[5,14] The layered structure consisting of alternating graphene sheets and polymer layers offered highly anisotropic characteristics to composites between two different directions of alignment and perpendicular to it in terms of mechanical properties, electrical conductivity, and gas/moisture barrier characteristics. Proper reduction of GO into rGO enhanced the stability of dispersion in the polymer matrix, giving rise to improved percolation threshold, mechanical, electrical, and thermal properties of the composites in the alignment direction.[4,14]

More recently, a three-dimensional (3D) interconnected graphene foam (GF) has gained much interest for application in various areas, especially as electrodes for high-performance batteries due to its excellent electrochemical capacities and an extremely large surface area with a low density.[15,16] Atomic carbon is chemical vapor deposited (CVD) on a porous Ni template to synthesize 3D GF, and the porous structure is preserved in GF after etching the Ni template. The 3D structural integrity and high electrical conductivity that a GF possesses make it an ideal filler material for polymer composites. A typical method to prepare GF/polymer composites is by infiltrating freestanding GF with different kinds of polymers, ultimately eliminating the problems associated with graphene agglomeration in polymers. However, the practical application of GF/polymer composites is still at its infant stage, and very few studies have appeared in the open literature reporting their properties. The electrical conductivity of GF/polydimethylsiloxane (PDMS) foam composite reached 2 S/cm, while the compressive strength of GF/epoxy composites showed a notable 55% improvement compared to neat epoxy.[17,18] Composites can also be prepared by infiltrating a prepolymer, typically epoxy resin, into the graphene grown on a Ni foam (G-Ni foam), followed by epoxy curing and dissolving the Ni foam template. The resultant GF/epoxy composite prepared in this way contained interconnected microscale voids created in place of the Ni template, forming an interconnected cellular structure.[19] Compared to the above solid GF composites, the cellular-structured composites are lighter and possess good liquid permeability, and the porous structure can potentially enhance the fracture toughness of the composites as in the porous polymer thin films.[20]

This paper reports the synthesis of interconnected porous GF/epoxy composites by impregnation of epoxy resin into the 3D G-Ni foam *via* CVD, followed by curing of the polymer and etching of the Ni template. The mechanical properties, fracture toughness, and transport properties of the composites were specifically evaluated. Special emphasis was placed on studying the toughening mechanisms of the composites arising from the interconnected graphene network structure with the voids created by removing the Ni template.

RESULTS AND DISCUSSION

GF Preparation and Characterization. A freestanding GF with a continuous and interconnected 3D network which was inherited from the structure of the original Ni template is shown in Figure 1a,b. Figure 1c presents a hollow wall structure of a broken foam end exposed after Ni etching. Due to its high porosity, the density of GF was 1.3 mg/cm^3 at a CH_4 concentration of 0.7 vol %. Figure 1d shows ripples with sizes in the range of submicrometer to several micrometers on the surface of GF. It was postulated that they were formed due to the different thermal expansion coefficients between the Ni template and graphene.[15] However, similar ripples or grain boundaries were also observed in graphene platelets exfoliated from the natural graphite flakes, suggesting the ripples were inherent to graphene.[21] These ripples may offer an additional mechanical interlocking mechanism with polymer chains, enhancing the interfacial adhesion.

Both monolayer and few-layer graphene were coexistent in the GF prepared in this study, indicating that the single Ni grain may have independently affected the precipitation of the graphene films during CVD. The transmission electron microscope (TEM) images and Raman spectra shown in Figures 1e and S1 (see Supporting Information) indicate that the GF grown at a CH_4 concentration of 1.4 vol % consisted of monolayer, bilayer, and few-layer graphene sheets with an average number of four. There are several important factors that affect the number of graphene layers in CVD-grown GF, including carbon source gas concentration, reaction temperature and time, cooling rate, and template materials.[15,22−24] Figure 1f shows an approximately linear relationship between CH_4 concentration, average number of graphene layers, and GF density. When the CH_4 concentration varied from 0.7 to 4.0 vol %, the number of graphene layers increased from 3 to 27 layers along with an increase of GF density from 1.3 to 6.8 mg/cm^3. Furthermore, the freestanding GF was free of nickel, as indicated by the X-ray photoelectron spectroscopy (XPS) spectrum and the TEM energy-dispersive X-ray (TEM-EDX) profile in Figure S2a,b (see Supporting Information), confirming that the process using hot hydrochloric acid (HCl) was sufficient to thoroughly remove the Ni template. The XPS survey spectrum of freestanding GF (Figure S2a) consisted of carbon and a trace amount of oxygen, the latter of which may originate from the adsorbed air onto the graphene surface or tiny PMMA residue.[25] No evidence of Ni 2p was noted at binding energies between 850 and 870 eV.[26]

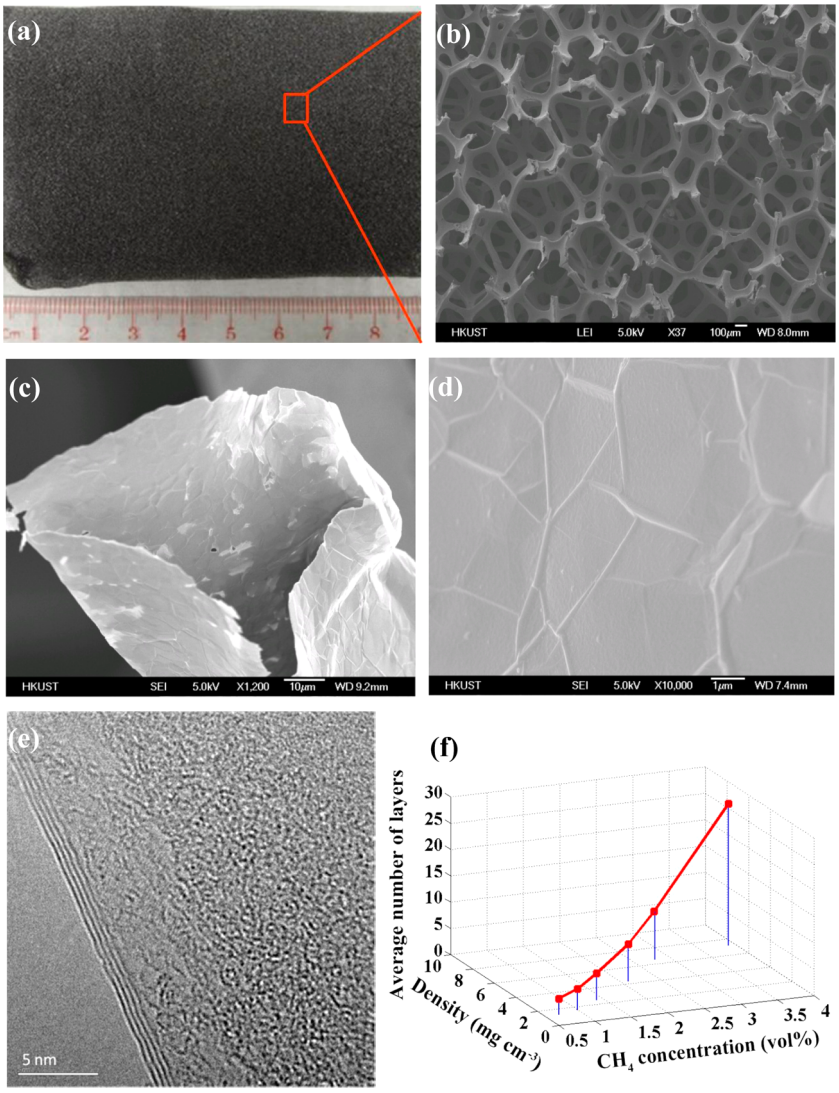

Figure 1. (a) Digital image and (b) SEM image of GF; (c) broken foam end and (d) magnified view of foam surface; (e) typical TEM image of GF prepared at a CH_4 concentration of 1.4 vol %; and (f) density and average number of graphene layers of GF as a function of CH_4 concentration used in CVD growth.

Porous Structure of GF/Epoxy Composites. The fabrication process for GF/epoxy composites consisted of three steps, as schematically illustrated in Figure 2: namely, (i) impregnation of diluted epoxy resin into the porous G-Ni foam to produce prepreg; (ii) evaporation of solvent and curing of epoxy; and (iii) etching of Ni template to create cellular-structured composites. Figure 3a shows a typical optical image of a polished cross section of the GF/epoxy composite containing 0.2 wt % GF. The microcellular pores were present between the nearly spherical blocks of epoxy in the form of curved triangular, dog-bone shapes, resembling the profile of the porous Ni template. These pores with average sizes in the range of tens to hundreds of micrometers were interconnected throughout the composite (see Figure 3b,c). The pore volume fraction estimated from the measured densities of the solid epoxy (1.19 g/cm^3) and GF/epoxy composites (0.96 g/cm^3) was 19.3 vol %. This value is consistent with the average value of 18.7 vol % obtained from the analysis of more than 30 micrographs of polished composite cross sections. Considering that the average thickness of the GF strut is only ~30 nm and assuming that the pressure applied during curing did not distort the Ni template structure, the pore volume in the "porous epoxy" without GF should be much similar to that in the composite.[27] Figure 3d indicates that the GF adhered well to the epoxy matrix, showing excellent resin permeability of the G-Ni foam due to the large surface area and the presence of interconnected pores. The area scanning from the SEM-EDX profile of the freeze-fractured cross section of GF/epoxy composites confirmed that there was no evidence of Ni residue left in the composite after etching (Figure S2d). The excess Cl came from the residual HCl, which can be removed by rinsing with deionized (DI) water.

Glass Transition Temperature and Electrical Properties. Glass transition temperature, T_g, is a measure of chain

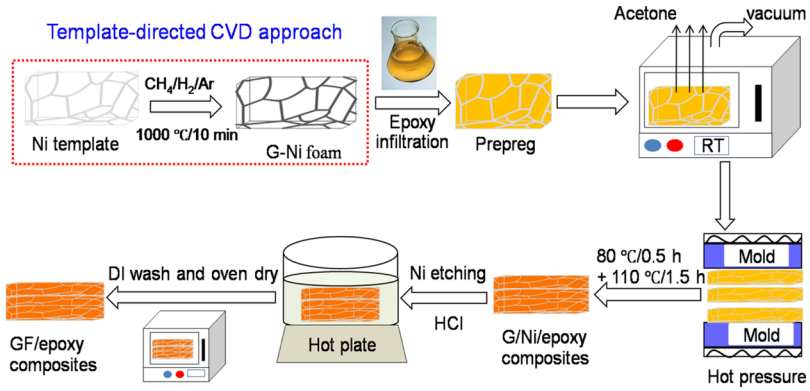

Figure 2. Flowchart for the preparation of GF/epoxy composites.

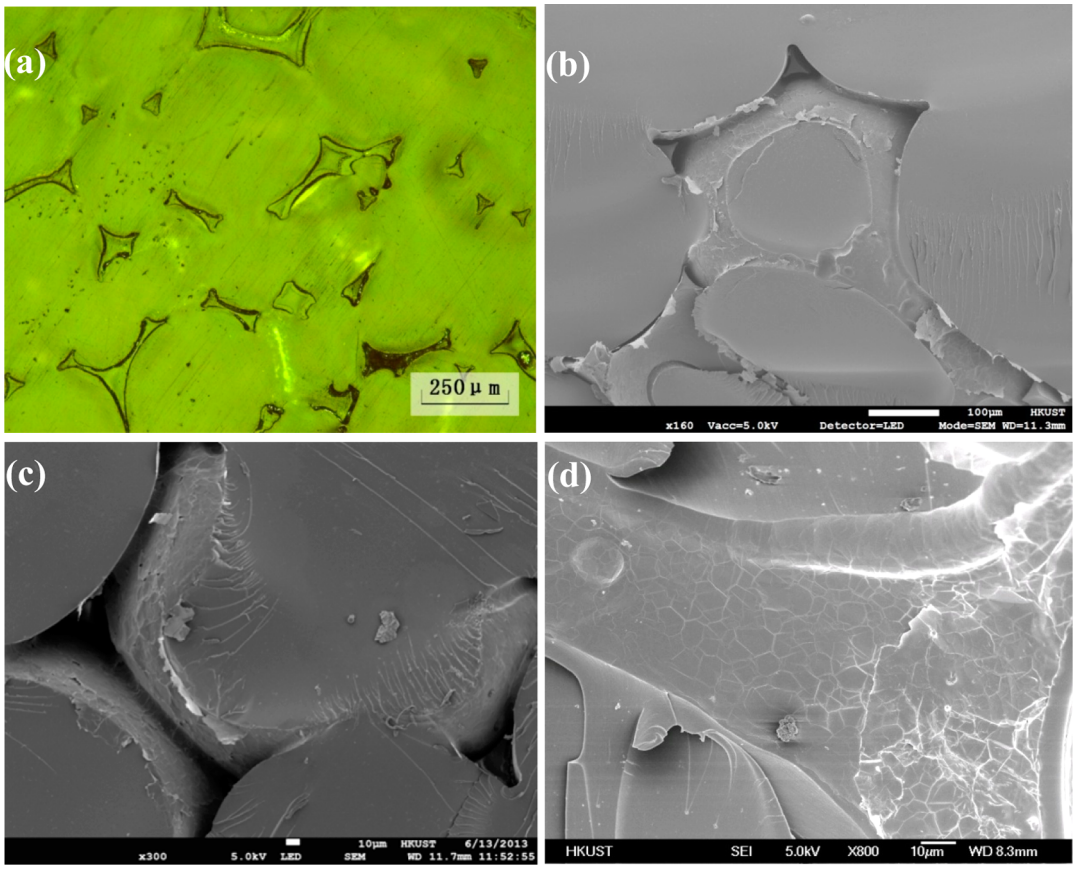

Figure 3. (a) Polished surface of a GF/epoxy composite showing pore distribution; (b–d) typical scanning electron microscope (SEM) images of GF/epoxy composites containing 0.2 wt % GF prepared at a CH_4 concentration of 1.4 vol %.

segment mobility and thermal stability of a polymer. Figures 4a and S3a (see Supporting Information) show that the T_g of the composites measured by DSC increased drastically from 94.9 to 126.2 °C with only 0.2 wt % GF, and the surge was followed by saturated values for GF contents beyond 0.2 wt %. The complementary dynamic mechanical analysis (DMA) measurements on selected GF/epoxy composites (Figure S3b) confirmed the remarkable T_g enhancements. While the general trends were very similar, the absolute values of T_g measured by DMA were slightly higher than the DSC results. The nearly identical T_g values for the solid and porous epoxy resins (black arrow in Figure S3a) indicate that the increase in T_g arose chiefly from the GF reinforcement into the epoxy. The extraordinary surge in T_g by 31 °C with 0.2 wt % GF has significant analogy with a recent report on 0.05 wt % functionalized graphene sheet (FGS) in PMMA composites as a result of the hindrance of molecular mobility in the vicinity of GF.[9] In addition, judging from our recent work on aligned rGO/epoxy composites where less than 20 °C increase in T_g was observed with 2.0 wt % rGO,[4] the 3D cellular GF appears to be much more efficient for improving the thermal stability of epoxy than the

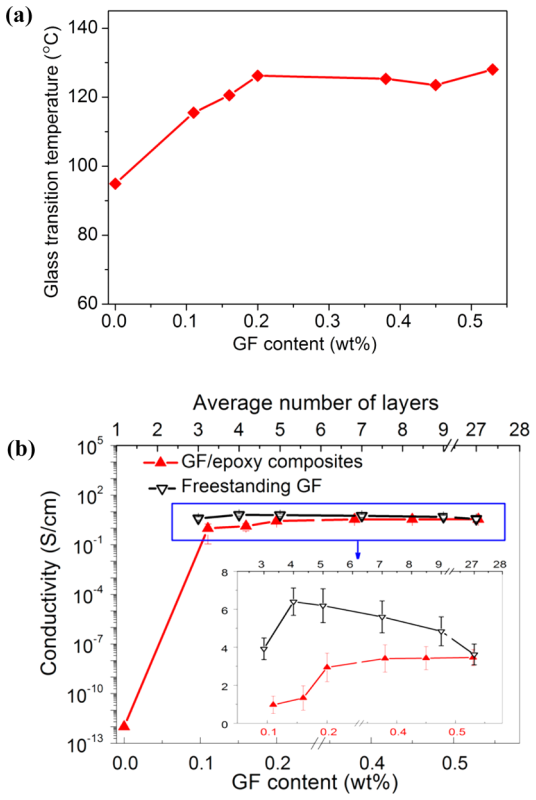

Figure 4. (a) Glass transition temperature and (b) electrical conductivity of GF/epoxy composites as a function of GF content. The conductivity of freestanding GF is superimposed in inset of (b).

individual, well-aligned rGO sheets. Improvement in T_g requires the interphase surrounding the nanofillers to interact with polymer so that the mobility of molecular chain segments is restricted.[28] Well-dispersed nanofillers and adequate interactions with the matrix polymer are the two prerequisites to a substantial increase in T_g. Based on the above discussion, the following factors are likely responsible for the efficient restriction of polymer mobility and augmented thermal stability, resulting in remarkable T_g enhancement. (i) The regularly spaced cellular structure of GF significantly boosted the interactions with epoxy while totally eliminating detrimental reagglomeration of graphene in the matrix.[29] (ii) The network structure of GF had a large surface area allowing interface contacts with the polymer matrix. This naturally created a substantial interphase region around the percolated GF where the mobility of the polymer chains was constrained.[28] (iii) The nanoscale surface roughness of GF with many ripples (see Figure 1d) likely resulted in enhanced mechanical interlocking with the polymer chains and consequently better interfacial adhesion,[30] which had a positive influence on thermal stability of the matrix. A similar effect has been suggested by previous molecular dynamics simulation, showing altered polymer chain dynamics because of the geometric constraints at the nanofiller surfaces.[31] Meanwhile, rheological percolation phenomenon or percolated interphase may be responsible for the saturation of T_g at higher graphene contents (red arrow in Figure S3a).[9,32] It appears that the polymer mobility in the composites was little affected by the increased number of graphene layers due to higher GF contents. Likewise, it is easy to understand why the percolation at 0.2 wt % GF in this study was higher than the reported 0.05 wt % for FGS/PMMA composites.

The high aspect ratio of graphene and exceptional electron mobility make it an attractive option to rival other conductive nanofillers, such as CNTs and metal nanowires, for the preparation of conductive polymer composites. Constructing a 3D interconnected network as the fast transport channel of charge carriers in the insulating polymer matrix is an efficient way of realizing rapid insulator-to-conductor transition and achieving excellent electrical conductivity.[33] Figure 4b shows an electrical conductivity of 10^{-12} S/cm for the neat epoxy resin, which is similar to reported values.[34] With the addition of 0.1 wt % GF, the electrical conductivity surged to 0.97 S/cm by 12 orders of magnitude, with a percolation occurring approximately at 0.05 wt % for the GF/epoxy composites. In view of the absence of residual Ni template in the freestanding GF and GF/epoxy composites (see Figure S2), the above significant gains in electrical conductivity can be ascribed to the incorporation of GF in the epoxy matrix. This conductivity value is at least 5 orders of magnitude higher than those of chemically derived graphene composites at graphene contents above percolation.[7,15] Possible reasons behind the much lower electrical conductivities of the latter composites include incomplete reduction of chemically derived GO and their inability to systematically form interconnected network limited by the small sizes and randomly distributed GO sheets in the polymer matrix. By contrast, the high electron mobility offered by the seamlessly interconnected 3D network of high-quality GF was responsible for the exceptional electrical conducting performance. In addition, the CVD-grown GF does not require usual reduction processes to restore the inherent conductivity of graphene.

The inset in Figure 4b indicates that the electrical conductivity of freestanding GF did not show a monotonic increase with the number of graphene layers and had a maximum conductivity of 6.4 S/cm with four layers of graphene, or 0.16 wt % GF in the composite. This observation is very similar to previous findings on CVD-grown GF and GF/PDMS composites where an optimal average number of graphene layer corresponding to the maximum conductivity was identified to be about five.[15] A further increase in GF content beyond 0.38 wt %, or about seven graphene layers, resulted in a rather saturated conductivity of the GF/epoxy composites. It is also interesting to note that the conductivity of freestanding GF was consistently higher than the GF/epoxy composites until they

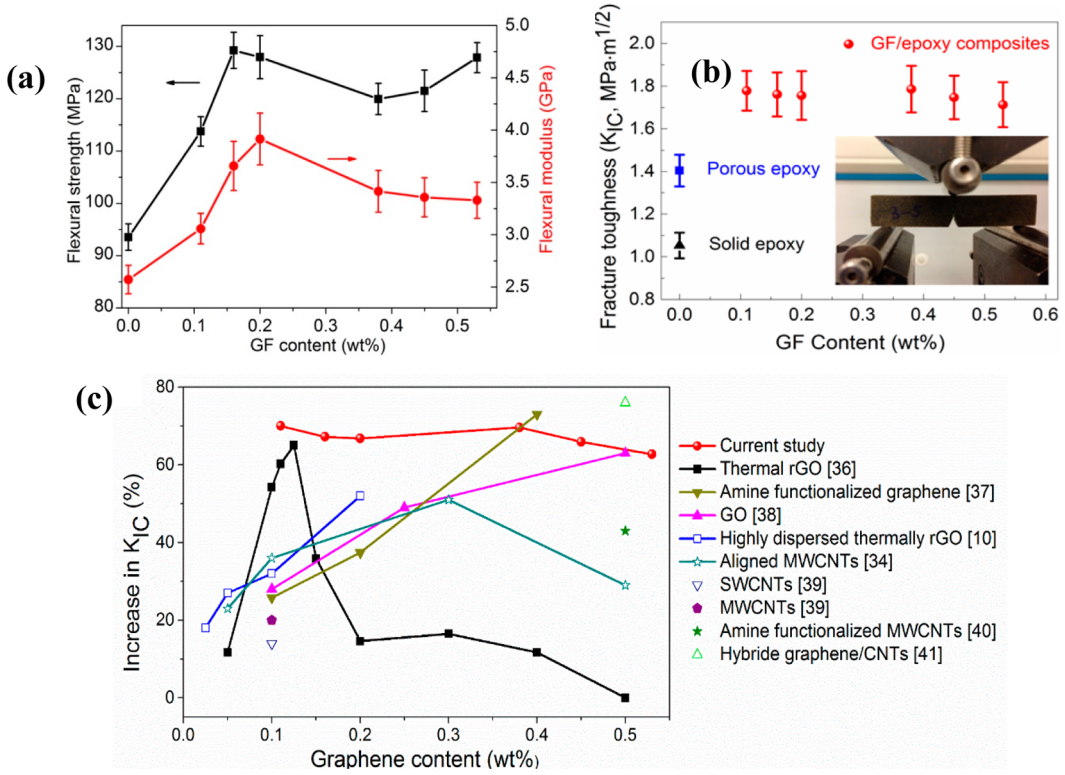

Figure 5. (a) Flexural strength and modulus of the solid epoxy and composites as a function of GF content; (b) mode I fracture toughness, K_{IC}, plotted as a function of GF content. The inset shows the fracture test of a SENB sample; and (c) comparison of fracture toughness between epoxy-based nanocomposites containing graphene and CNTs taken from literature.

gradually converged at higher GF contents, suspecting minor damage to the conducting structure of the GF at low contents during the epoxy infiltration and curing at a high temperature.

Flexural Properties and Fracture Toughness. Incorporation of GF into the epoxy system also significantly increased both the flexural modulus and strength compared to the solid neat epoxy, as shown in Figure 5a. These properties showed maxima at ~0.2 wt % GF with 53 and 38% improvements, respectively, followed by moderate reductions with further increase in GF content—a functionally similar characteristic to T_g (see Figure 4a). This finding signifies that the rheological percolation threshold of GF positively affects not only the T_g but also the flexural properties of the GF/epoxy composites. It is well-known that the composite modulus is dependent on the modulus and volume fraction of the composite constituents, whereas the strength is also influenced by the filler−matrix interfacial adhesion.[35] This may explain the relatively moderate improvement of the flexural strength because the GF surface was not specifically functionalized. Figure 5b shows the fracture toughness, K_{IC}, of the solid epoxy is ~1.05 MPa·m$^{1/2}$, which is consistent with the published values for a similar epoxy system.[36] The K_{IC} value increased sharply to 1.78 MPa·m$^{1/2}$ at 0.1 wt % GF, corresponding to a remarkable enhancement of 70% compared to the solid epoxy. There was an apparent plateau or marginal reductions with further increase in GF content, probably because the increased graphene layers only led to slippage between adjacent layers to disrupt the weak van der Waals forces when the composites were subjected to an external load.[10] Surprisingly, the "porous epoxy" prepared from the Ni foam/epoxy composites by etching out Ni showed a moderate value K_{IC} = 1.41 MPa·m$^{1/2}$, about 34% higher than that of the solid epoxy, indicating substantial toughening mechanisms offered by the pores created after removing the Ni template.

To identify the benefits of GF reinforcement, fracture toughness K_{IC} values of epoxy-based nanocomposites containing graphene sheets and CNTs taken from the literature are compared with the present study in Figure 5c and Table S1 (see Supporting Information). Due to the large variations in K_{IC} of solid epoxy resins from 0.5 to 1.63 MPa·m$^{1/2}$,[10,37] the increment of fracture toughness of composites compared to their respective control solid epoxy is reported here. Among many CNT/epoxy composites, the best reported enhancement in K_{IC} was 51% at 0.3 wt % of aligned MWCNTs.[34] However, the K_{IC} of SWCNT/epoxy composites was rather disappointing, delivering 14% improvement with 0.1 wt % SWCNT.[39] The performance of the composites containing graphene was impressive especially when the graphene sheets were preferentially aligned. The maximum reported increase in K_{IC} for rGO/epoxy was 65% at 0.125 wt %.[36]

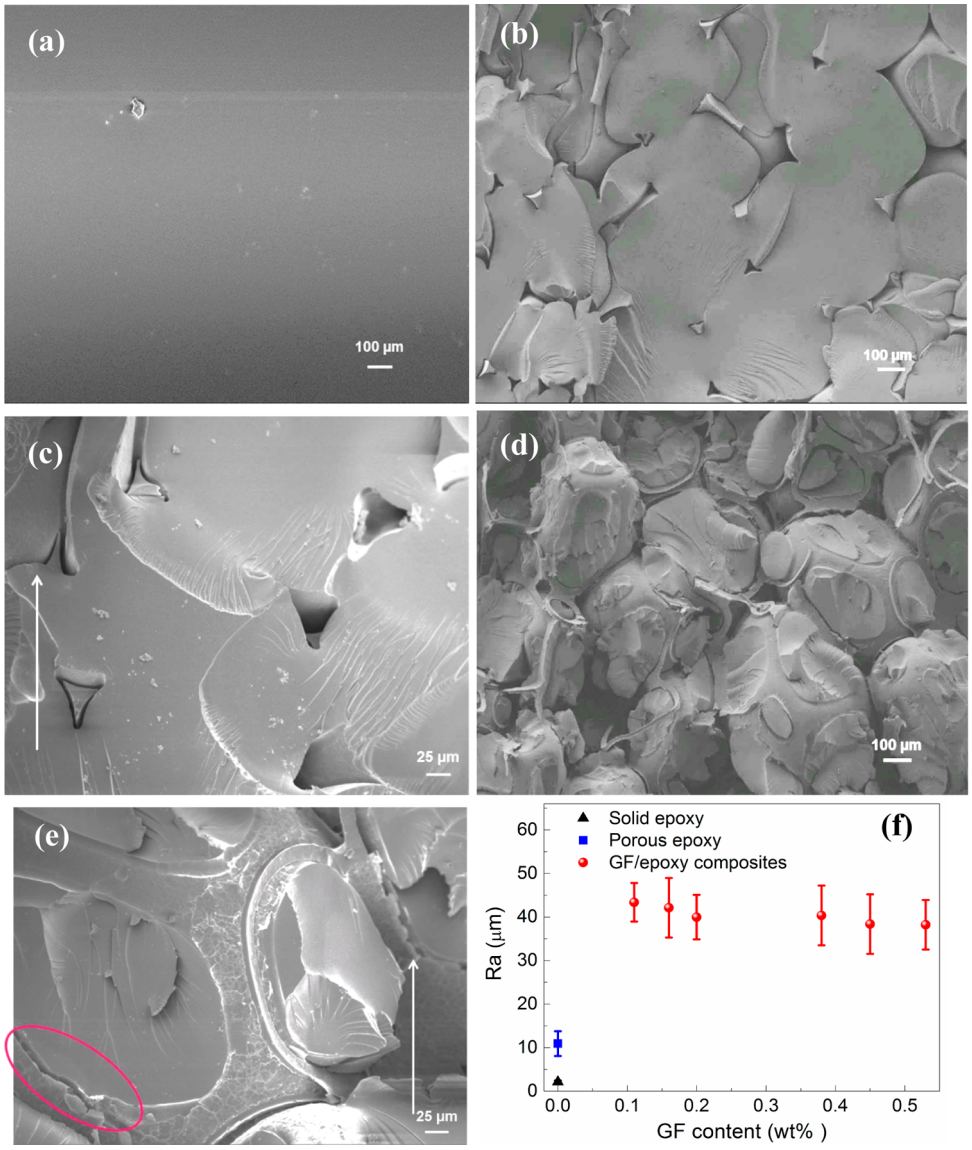

Figure 6. SEM images of quasi-static fracture surfaces of (a) solid epoxy, (b,c) porous epoxy, and (d,e) GF/epoxy composites with 0.1 wt % GF; (f) fracture surface roughness of samples as a function of GF content. White arrows in (c) and (e) indicate crack propagation direction.

However, improvements were largely impaired at rGO contents higher than 0.125 wt % due to the deteriorated filler dispersion. The corresponding performance of GF/epoxy composites was among the best for all graphene contents and was much better than the GO and rGO counterparts.

The above comparison clearly indicates that the reinforcement with 3D interconnected GF is much more effective in improving the fracture toughness of composites than 1D CNTs, 2D GO, or rGO sheets. There are several reasons behind this conclusion: namely, (i) the integrated 3D structure of GF can totally eliminate the issues of uniform dispersion of CNTs or GO sheets prior to incorporation into the polymer, and reagglomeration or restacking after addition into the polymer; (ii) the resulting properties of 3D GF/polymer composites are less sensitive to surface functionalization than for the composites based on CNTs or 2D GO sheets; and (iii) the 3D GF can play much the same role as 3D fabrics play in eliminating the interlaminar planes and the associated premature failures in textile composites reinforced with braided or 3D woven fabrics. In particular, the total elimination of nanofiller dispersion problems without additional functionalization can open up new manufacturing processes to produce advanced nanocomposites containing higher nanofiller contents than the current technology can offer. The 3D textile composites have been extensively applied to produce composite components where delamination failures have to be totally avoided.

Toughening Mechanisms. Examination of the fracture surfaces of the solid epoxy, the "porous" epoxy, and the GF/epoxy composite specimens revealed well-defined distinctions between them, as shown in Figure 6.

The solid epoxy showed featureless and smooth, typically brittle surface (Figure 6a), indicating very weak resistance to crack propagation. Compared to the mirror-like fracture surface of solid epoxy, the porous epoxy presented a rough surface due to the crack propagation at different planes with several steps. The fracture surface featured irregular-shaped epoxy blocks partly separated by characteristic triangular pore structures (Figure 6b,c). These pores are the traces of the original Ni templates, which functioned as hollow particles (i) to induce local crack tip blunting by changing the stress state from the plane strain to the plane stress condition and (ii) to form microcracking/bifurcation dilatation fracture process zone.[42,43] The fine river markings (Figure 6c) occurred mainly at the slopes and boundaries between two different planes, suggesting crack growth by matrix shearing which was promoted by the triangular pores as the crack front passed through them.

The typical fracture surface of GF/epoxy composites presents coarse, multiplane features with numerous protuberances of their sizes equivalent to the spherical cells between the GF network (Figure 6d,e). The examination of many fracture surfaces in addition to those shown here failed to identify clear evidence of crack pinning—a largely expected toughening mechanism to occur in the composite. Crack pinning is one of the most important failure mechanisms in rigid particulate-reinforced composites and is normally manifested by crack front bowing and the formation of tails,[36,38] which were totally absent in the present GF/epoxy composite. Thus, it is concluded that crack pinning did not prevail in composites with hollow GF network because GF tended to collapse upon being impinged by the advancing cracks, instead of allowing crack front bowing. Therefore, the major roles of the GF reinforcement in improving the fracture toughness of epoxy matrix can be ascribed to the following. (i) The crack tips are blunted by the seamlessly interconnected walls of GF before collapse to induce winding crack tip deflections. As a result, they tend to tilt, twist, or bifurcate along the boundary of GF under mixed modes of tension and shear to form mound-shaped crack paths through the epoxy matrix in their wakes. Thus, the crack propagation under the mixed-mode condition resulted in the formation of protuberances with a much increased fracture surface area after the collapse of GF reinforcements (Figure 6d), requiring a higher energy absorption than in pure mode I tension.[36] (ii) During the above crack tip blunting process, the GF/epoxy interphase can be debonded due to the moderate interfacial adhesion along the boundary of GF without any functionalization, as indicated by the circle (Figure 6e). The interfacial debonding can contribute to enhanced energy absorption in the composite.[44] (iii) When the crack tip meets the edges of the GF, slippage and separation occur between the adjacent graphene layers due to the disruption of the weak van der Waals forces between them, thus contributing to more energy absorption.[10]

To fully understand the fracture mechanisms and thus to quantitatively correlate the change in fracture surface morphology from the mirror-like planar to rugged surface with the increase in fracture toughness, the fracture surface roughness was measured, as shown in Figure 6f. It is well-known that the toughening of composites due to crack tip blunting and deflection often result in significantly enhanced surface roughness.[45] The results indicate that there was an almost 20-fold upsurge in average surface roughness when the epoxy resin was reinforced with only 0.1 wt % GF. The surface roughening began to saturate with further increase in the GF content above 0.1 wt %. It is worth noting that there was significant functional analogy between the fracture toughness (Figure 5b) and the fracture surface roughness (Figure 6f) with respect to GF content. This finding further confirms the important role that the fracture surface roughness played in determining the fracture toughness of the composite. Very similar observations with comparable conclusions were also reported for FGS/epoxy composites and silane-treated MWCNTs/epoxy composites.[36,46] In summary, the porous GF reinforcement effectively blunted the advancing cracks, facilitating crack tip deflection with a rougher fracture surface and a larger surface area, which in turn improved the fracture toughness of the composite.

CONCLUSION

The present study reports the growth of a 3D interconnected GF on a porous Ni template *via* the CVD method. Cellular-structured GF/epoxy composites were fabricated using the 3D GF based on a three-step fabrication process. It involved (i) impregnation of epoxy resin into the porous G-Ni foam to produce prepreg; (ii) evaporation of solvent and curing; and (iii) etching of Ni template to form composites with an interconnected porous GF network and high structural integrity. The following can be highlighted from the experimental study. The freestanding, ultralight, and defect-free 3D porous GF presented hollow wall structures and ripples on the surface. There existed a linear relationship between the CH_4 concentration, average number of graphene layers, and GF density. The GF/epoxy composites had a density of 0.96 g/cm^3 and an average pore volume fraction of ~19 vol %. A remarkable electrical conductivity of 3 S/cm was delivered at 0.2 wt % GF, and a low percolation threshold of 0.05 wt % was achieved owing to the 3D integrated GF structure. There was a notable increase of T_g by 31 °C, along with 53 and 38% enhancements in flexural modulus and strength at ~0.2 wt % GF, respectively. These properties were shown saturated at higher GF contents where the rheological percolation

phenomenon or percolated interphase occurred. A remarkable 70% enhancement in fracture toughness of the composites compared to the solid epoxy was achieved at 0.1 wt % GF content. Crack tip blunting and deflection due to the porous GF network functioning as crack arresters and crack propagation under mixed-mode condition, resulting in a rougher fracture surface and a larger surface area, were responsible for the enhanced fracture toughness. In summary, it is challenging to design materials with concurrent improvements in both strength and fracture toughness because they are often mutually exclusive and, in most cases, one property is sacrificed for the sake of the other.[35] However, we demonstrated in this work that significant improvements in both modulus/strength and fracture toughness were achieved by introducing a small amount of GF into an epoxy matrix. There is a significant analogy between the composites reinforced by 3D GF and 3D textile composites in terms of their capability to suppress crack propagation through the thickness of the composites, especially under delamination and impact modes of loading, due to the 3D nature of interconnected reinforcement structure.

EXPERIMENTAL SECTION

Preparation of GF/Epoxy Composites. G-Ni foam was prepared by CVD. The details can be found in the Supporting Information. The epoxy resin (LY1556, supplied by Huntsman Advanced Materials) was diluted with acetone at a weight ratio of 20:100 of epoxy, and the curing agent, triethylenetetramine, was added at a weight ratio of 12:100 of epoxy. The G-Ni foam was immersed into the diluted epoxy resin system for 0.5 h to form a prepreg which was subsequently degassed in a vacuum oven at room temperature (RT) for 5 h to evaporate acetone and eliminate the entrapped air. A desired number of prepreg layers were stacked in an aluminum mold and hot-pressed at 80 °C for 0.5 h at a pressure of 0.5 MPa to remove excess resin, followed by further curing at 110 °C for 1.5 h. The Ni template was removed by immersing the cured composites into concentrated HCl (3 M) at 80 °C for 48 h. After being rinsed with DI, the composites were further treated at 120 °C for 2 h to eliminate any stresses arising from the chemical etching and were slowly cooled to RT in the furnace. The composites produced thereby contained GF in the range from 0.1 to 0.53 wt %.

For comparison of the properties with those of the GF/epoxy composites, the Ni template without graphene layers was impregnated with the same epoxy resin system and cured employing the same procedure as above. The Ni template was etched similarly to produce rectangular plates of neat epoxy containing voids created in place of Ni template, which was designated as "porous epoxy" with an average pore volume of ~19 vol %.

Characterization. Various microscopes, including an optical microscope (Olympus BX51M), a SEM (JEOL JSM-6700F) with a 5 kV accelerating voltage, a SEM-EDX (JEOL JSM-6390) with a 15 kV accelerating voltage, and a field emission TEM (FETEM, JEOL 2010F) at an acceleration voltage of 200 kV, were used to characterize the morphologies and the elemental maps of GF and GF/epoxy composites. The surface roughness, R_a, of the fracture surface was determined using the optical surface profiler (Profilometer Tencor Alpha Step 200). At least 10 scans of 2×2 mm^2 square were taken of each sample. XPS (Axis Ultra DLD) was used to characterize the elemental compositions of freestanding GF. The structure of GF was evaluated on a micro-Raman spectrometer (Renishaw micro-Raman/photoluminescence system) with Ar laser excitation at 514.5 nm wavelength. The electrical conductivity was measured based on the four-point probe method using a resistivity/Hall measurement system (Scientific Equipment & Services). To reduce the contact resistance between the probes and the composite surface, the contact points were coated with silver paste. The glass transition temperatures, T_g, of the solid epoxy and the GF/epoxy composites were characterized by a modulated differential scanning calorimeter (DSC, QA1000, TA Instruments). Measurements were conducted at a ramp rate of 10 °C/min in a nitrogen atmosphere. Complementary DMA (DMA 7-PerkinElmer) was also performed at a constant heating rate of 3 °C/min from 25 to 180 °C and at 1 Hz. The details for flexural properties and fracture toughness tests can be found in the Supporting Information.

Conflict of Interest: The authors declare no competing financial interest.

Acknowledgment. The project was supported by the Research Grants Council of Hong Kong SAR (project codes: 614010, 613811) and the Australian Research Council (Discovery Project DP130104648). Technical assistance from the Materials Characterization and Preparation Facilities (MCPF) and Advanced Engineering Materials Facilities (AEMF), HKUST, is appreciated. We also wish to thank X. Du and H. Liu for valuable discussions.

Supporting Information Available: The materials and process parameters for synthesis G-Ni foam in CVD, TEM images, Raman and XPS spectra and TEM-EDX profile of GF, SEM-EDX image, DSC and DMA tan δ curves, and tabulated fracture toughness of GF/epoxy composites, as well as flexural properties and fracture toughness measurements are included. This material is available free of charge *via* the Internet at http://pubs.acs.org.

REFERENCES AND NOTES

1. Zhu, Y.; Murali, S.; Cai, W.; Li, X.; Suk, J. W.; Potts, J. R.; Ruoff, R. S. Graphene and Graphene Oxide: Synthesis, Properties, and Applications. *Adv. Mater.* **2010**, *22*, 3906–3924.
2. Geim, A. K.; Novoselov, K. S. The Rise of Graphene. *Nat. Mater.* **2007**, *6*, 183–191.
3. Lee, C.; Wei, X.; Kysar, J. W.; Hone, J. Measurement of the Elastic Properties and Intrinsic Strength of Monolayer Graphene. *Science* **2008**, *321*, 385–388.
4. Yousefi, N.; Lin, X.; Zheng, Q.; Shen, X.; Pothnis, J. R.; Jia, J.; Zussman, E.; Kim, J. K. Simultaneous *In Situ* Reduction, Self-Alignment and Covalent Bonding in Graphene Oxide/Epoxy Composites. *Carbon* **2013**, *59*, 406–417.
5. Yousefi, N.; Gudarzi, M. M.; Zheng, Q.; Aboutalebi, S. H.; Sharif, F.; Kim, J. K. Self-Alignment and High Electrical Conductivity of Ultralarge Graphene Oxide−Polyurethane Nanocomposites. *J. Mater. Chem.* **2012**, *22*, 12709–12717.
6. Kim, H.; Macosko, C. W. Processing-Property Relationships of Polycarbonate/Graphene Composites. *Polymer* **2009**, *50*, 3797–3809.
7. Stankovich, S.; Dikin, D. A.; Dommett, G. H. B.; Kohlhaas, K. M.; Zimney, E. J.; Stach, E. A.; Piner, R. D.; Nguyen, S. T.; Ruoff, R. S. Graphene-Based Composite Materials. *Nature* **2006**, *442*, 282–286.
8. Feng, X. M.; Li, R. M.; Ma, Y. W.; Chen, R. F.; Shi, N. E.; Fan, Q. L.; Huang, W. One-Step Electrochemical Synthesis of Graphene/Polyaniline Composite Film and Its Applications. *Adv. Funct. Mater.* **2011**, *21*, 2989–2996.
9. Ramanathan, T.; Abdala, A. A.; Stankovich, S.; Dikin, D. A.; Herrera-Alonso, M.; Piner, R. D.; Adamson, D. H.; Schniepp, H. C.; Chen, X.; Ruoff, R. S.; *et al.* Functionalized Graphene Sheets for Polymer Nanocomposites. *Nat. Nanotechnol.* **2008**, *3*, 327–331.
10. Tang, L. C.; Wan, Y. J.; Yan, D.; Pei, Y. B.; Zhao, L.; Li, Y. B.; Wu, L. B.; Jiang, J. X.; Lai, G. Q. The Effect of Graphene Dispersion

on the Mechanical Properties of Graphene/Epoxy Composites. *Carbon* **2013**, *60*, 16–27.
11. Bai, H.; Li, C.; Shi, G. Functional Composite Materials Based on Chemically Converted Graphene. *Adv. Mater.* **2011**, *23*, 1089–1115.
12. Lin, X.; Shen, X.; Zheng, Q.; Yousefi, N.; Ye, L.; Mai, Y. W.; Kim, J. K. Fabrication of Highly-Aligned, Conductive, and Strong Graphene Papers Using Ultralarge Graphene Oxide Sheets. *ACS Nano* **2012**, *6*, 10708–10719.
13. Gao, Y.; Liu, L. Q.; Zu, S. Z.; Peng, K.; Zhou, D.; Han, B. H.; Zhang, Z. The Effect of Interlayer Adhesion on the Mechanical Behaviors of Macroscopic Graphene Oxide Papers. *ACS Nano* **2011**, *5*, 2134–2141.
14. Yousefi, N.; Gudarzi, M. M.; Zheng, Q.; Lin, X.; Shen, X.; Jia, J.; Sharif, F.; Kim, J. K. Highly Aligned, Ultralarge-Size Reduced Graphene Oxide/Polyurethane Nanocomposites: Mechanical Properties and Moisture Permeability. *Composites, Part A* **2013**, *49*, 42–50.
15. Chen, Z.; Ren, W.; Gao, L.; Liu, B.; Pei, S.; Cheng, H. M. Three-Dimensional Flexible and Conductive Interconnected Graphene Networks Grown by Chemical Vapour Deposition. *Nat. Mater.* **2011**, *10*, 424–428.
16. Ji, H.; Zhang, L.; Pettes, M. T.; Li, H.; Chen, S.; Shi, L.; Piner, R.; Ruoff, R. S. Ultrathin Graphite Foam: A Three-Dimensional Conductive Network for Battery Electrodes. *Nano Lett.* **2012**, *12*, 2446–2451.
17. Chen, Z.; Xu, C.; Ma, C.; Ren, W.; Cheng, H. M. Lightweight and Flexible Graphene Foam Composites for High-Performance Electromagnetic Interference Shielding. *Adv. Mater.* **2013**, *25*, 1296–1300.
18. Chen, X.; Lu, Y.; Zhang, X.; Zhao, F. The Thermal and Mechanical Properties of Graphite Foam-Epoxy Resin Composites. *Mater. Des.* **2012**, *40*, 497–501.
19. Li, X.; Sun, P.; Fan, L.; Zhu, M.; Wang, K.; Zhong, M.; Wei, J.; Wu, D.; Cheng, Y.; Zhu, H. Multifunctional Graphene Woven Fabrics. *Sci. Rep.* **2012**, *2*, 1–8.
20. Kearney, A. V.; Litteken, C. S.; Mohler, C. E.; Mills, M. E.; Dauskardt, R. H. Pore Size Scaling for Enhanced Fracture Resistance of Nanoporous Polymer Thin Films. *Acta Mater.* **2008**, *56*, 5946–5953.
21. Li, J.; Sham, M. L.; Kim, J. K.; Marom, G. Morphology and Properties of UV/Ozone Treated Graphite Nanoplatelet/Epoxy Nanocomposites. *Compos. Sci. Technol.* **2007**, *67*, 296–305.
22. Li, X.; Magnuson, C. W.; Venugopal, A.; An, J.; Suk, J. W.; Han, B.; Borysiak, M.; Cai, W.; Velamakanni, A.; Zhu, Y.; *et al.* Graphene Films with Large Domain Size by a Two-Step Chemical Vapor Deposition Process. *Nano Lett.* **2010**, *10*, 4328–4334.
23. Miyata, Y.; Kamon, K.; Ohashi, K.; Kitaura, R.; Yoshimura, M.; Shinohara, H. A Simple Alcohol-Chemical Vapor Deposition Synthesis of Single-Layer Graphenes Using Flash Cooling. *Appl. Phys. Lett.* **2010**, *96*, 263105.
24. Reina, A.; Jia, X.; Ho, J.; Nezich, D.; Son, H.; Bulovic, V.; Dresselhaus, M. S.; Kong, J. Large Area, Few-Layer Graphene Films on Arbitrary Substrates by Chemical Vapor Deposition. *Nano Lett.* **2009**, *9*, 30–35.
25. Kim, K. S.; Lee, H. J.; Lee, C.; Lee, S. K.; Jang, H.; Ahn, J. H.; Kim, J. H.; Lee, H. J. Chemical Vapor Deposition-Grown Graphene: The Thinnest Solid Lubricant. *ACS Nano* **2011**, *5*, 5107–5114.
26. Chen, T.; Deng, F.; Zhu, J.; Chen, C.; Sun, G.; Ma, S.; Yang, X. Hexagonal and Cubic Ni Nanocrystals Grown on Graphene: Phase-Controlled Synthesis, Characterization and Their Enhanced Microwave Absorption Properties. *J. Mater. Chem.* **2012**, *22*, 15190–15197.
27. Zhang, X.; Yeung, K. K.; Gao, Z.; Li, J.; Sun, H.; Xu, H.; Zhang, K.; Zhang, M.; Chen, Z.; Yuen, M. M. F.; *et al.* Exceptional Thermal Interface Properties of a Three-Dimensional Graphene Foam. *Carbon* **2014**, *66*, 201–209.
28. Bansal, A.; Yang, H.; Li, C.; Cho, K.; Benicewicz, B. C.; Kumar, S. K.; Schadler, L. S. Quantitative Equivalence between Polymer Nanocomposites and Thin Polymer Films. *Nat. Mater.* **2005**, *4*, 693–698.
29. Rittigstein, P.; Priestley, R. D.; Broadbelt, L. J.; Torkelson, J. M. Model Polymer Nanocomposites Provide an Understanding of Confinement Effects in Real Nanocomposites. *Nat. Mater.* **2007**, *6*, 278–282.
30. Fang, M.; Wang, K.; Lu, H.; Yang, Y.; Nutt, S. Covalent Polymer Functionalization of Graphene Nanosheets and Mechanical Properties of Composites. *J. Mater. Chem.* **2009**, *19*, 7098–7105.
31. Xu, Z.; Buehler, M. J. Geometry Controls Conformation of Graphene Sheets: Membranes, Ribbons, and Scrolls. *ACS Nano* **2010**, *4*, 3869–3876.
32. Kota, A. K.; Cipriano, B. H.; Duesterberg, M. K.; Gershon, A. L.; Powell, D.; Raghavan, S. R.; Bruck, H. A. Electrical and Rheological Percolation in Polystyrene/MWCNT Nanocomposites. *Macromolecules* **2007**, *40*, 7400–7406.
33. Li, J.; Ma, P. C.; Chow, W. S.; To, C. K.; Tang, B. Z.; Kim, J. K. Correlations between Percolation Threshold, Dispersion State, and Aspect Ratio of Carbon Nanotubes. *Adv. Funct. Mater.* **2007**, *17*, 3207–3215.
34. Khan, S. U.; Pothnis, J. R.; Kim, J. K. Effects of Carbon Nanotube Alignment on Electrical and Mechanical Properties of Epoxy Nanocomposites. *Composites, Part A* **2013**, *49*, 26–34.
35. Kim, J. K.; Mai, Y. W. *Engineered Interfaces in Fiber Reinforced Composites*; Elsevier: Oxford, 1998; p 185.
36. Rafiee, M. A.; Rafiee, J.; Srivastava, I.; Wang, Z.; Song, H.; Yu, Z. Z.; Koratkar, N. Fracture and Fatigue in Graphene Nanocomposites. *Small* **2010**, *6*, 179–183.
37. Fang, M.; Zhang, Z.; Li, J.; Zhang, H.; Lu, H.; Yang, Y. Constructing Hierarchically Structured Interphases for Strong and Tough Epoxy Nanocomposites by Amine-Rich Graphene Surfaces. *J. Mater. Chem.* **2010**, *20*, 9635–9643.
38. Bortz, D. R.; Heras, E. G.; Martin-Gullon, I. Impressive Fatigue Life and Fracture Toughness Improvements in Graphene Oxide/Epoxy Composites. *Macromolecules* **2012**, *45*, 238–245.
39. Rafiee, M. A.; Rafiee, J.; Wang, Z.; Song, H.; Yu, Z. Z.; Koratkar, N. Enhanced Mechanical Properties of Nanocomposites at Low Graphene Content. *ACS Nano* **2009**, *3*, 3884–3890.
40. Gojny, F. H.; Wichmann, M. H. G.; Fiedler, B.; Schulte, K. Influence of Different Carbon Nanotubes on the Mechanical Properties of Epoxy Matrix Composites—A Comparative Study. *Compos. Sci. Technol.* **2005**, *65*, 2300–2313.
41. Chatterjee, S.; Nafezarefi, F.; Tai, N. H.; Schlagenhauf, L.; Nüesch, F. A.; Chu, B. T. T. Size and Synergy Effects of Nanofiller Hybrids Including Graphene Nanoplatelets and Carbon Nanotubes in Mechanical Properties of Epoxy Composites. *Carbon* **2012**, *50*, 5380–5386.
42. Leguillon, D.; Piat, R. Fracture of Porous Materials—Influence of the Pore Size. *Eng. Fract. Mech.* **2008**, *75*, 1840–1853.
43. Ke, Y. B.; Cotterell, B.; Mai, Y. W. The Fracture Resistance of Sintered Steel. *Mater. Sci. Eng., A* **1989**, *117*, 149–156.
44. Silva, R. V.; Spinelli, D.; Bosefilho, W. W.; Claroneto, S.; Chierice, G. O.; Tarpani, J. R. Fracture Toughness of Natural Fibers/Castor Oil Polyurethane Composites. *Compos. Sci. Technol.* **2006**, *66*, 1328–1335.
45. Garg, A. C.; Mai, Y. W. Failure Mechanisms in Toughened Epoxy Resins—A Review. *Compos. Sci. Technol.* **1988**, *31*, 179–223.
46. Ma, P. C.; Kim, J. K.; Tang, B. Z. Effects of Silane Functionalization on the Properties of Carbon Nanotube/Epoxy Nanocomposites. *Compos. Sci. Technol.* **2007**, *67*, 2965–2972.